Chin. Geogra. Sci. 2023 Vol. 33 No. 2 pp. 377−392
https://doi.org/10.1007/s11769-023-1337-1

Springer Science Press
www.springerlink.com/content/1002-0063

Spatiotemporal Changes in NDVI and Its Driving Factors in the Kherlen River Basin

YU Shan[1, 2], DU Wala[3], ZHANG Xiang[1, 2], HONG Ying[1, 2], LIU Yang[1, 2], HONG Mei[1, 2], CHEN Siyu[4]

(1. *College of Geographic Science*, *Inner Mongolia Normal University*, *Hohhot* 010022, *China*; 2. *Inner Mongolia Key Laboratory of Remote Sensing and Geographic Information Systems*, *Hohhot* 010022, *China*; 3. *Institute of Grassland Research*, *Chinese Academy of Agricultural Sciences*, *Hohhot* 010000, *China*; 4. *College of Science*, *Inner Mongolia University of Technology*, *Hohhot* 010051, *China*)

Abstract: Vegetation is an important factor linking the atmosphere, water, soil, and biological functions, and it plays a specific role in the climate change response and sustainable development of regional economies. However, little information is available on vegetation vulnerability and its driving mechanism. Therefore, studying temporal and spatial change characteristics of vegetation and their corresponding mechanisms is important for assessing ecosystem stability and formulating ecological policies in the Kherlen River Basin. We used Moderate-resolution Imaging Spectroradiometer (MODIS) normalized difference vegetation index (NDVI) remote sensing images from 2000 to 2020 to analyse temporal changes in NDVI with the autoregressive moving average model (ARMA) and the breaks for additive season trend (BFAST) in the basin and to assess natural, anthropogenic and topographic factors with the Geodetector model. The results show that: 1) the long NDVI time series remained stable in the Kherlen River Basin from 2000 to 2020, with a certain significant mutation period from 2013 to 2017; 2) the coefficient of variation (CV) in the analysis of the spatial NDVI was generally constant, mainly at the level of 0.01–0.07, and the spatial NDVI change was minimally impacted by external interference; and 3) temperature and precipitation are the key factors affecting the NDVI in the basin, and changes in local hydrothermal conditions directly affect the local NDVI. The results of this study could provide a scientific basis for the effective protection of the ecological environment and will aid in understanding the influence of vegetation change mechanisms and the corresponding factors.

Keywords: normalized difference vegetation index (NDVI); spatial stability; vegetation; ecology; Geodetector; Kherlen River Basin

Citation: YU Shan, DU Wala, ZHANG Xiang, HONG Ying, LIU Yang, HONG Mei, CHEN Siyu, 2023. Spatiotemporal Changes in NDVI and Its Driving Factors in the Kherlen River Basin. *Chinese Geographical Science*, 33(2): 377−392. https://doi.org/10.1007/s11769-023-1337-1

1 Introduction

Vegetation is the main body of the terrestrial ecosystem, plays an important role in the material and energy cycles of the atmosphere, hydrosphere and biosphere (Kim et al., 2011; Eisavi et al., 2015). Additionally, vegetation effect on carbon sink in the carbon cycle and can improve the ecological environment to a certain extent (Gottfried et al., 2012; Liu et al., 2017a). A vegetation index can accurately reflect information about land vegetation cover and are commonly employed as key indicators of land vegetation change. Furthermore, vegetation indices are critical for researching hydrological, ecological, and climate changes (Goward et al., 2002;

Received date: 2022-01-21; accepted date: 2022-06-10
Foundation item: Under the auspices of Project of Inner Mongolia Normal University to Introduce High-level Talents to Start Scientific Research (No. 1004021709), Key Special Project of Inner Mongolia (No. 2020ZD0028), Science and Technology Planning Project of Inner Mongolia Autonomous Region (No. 2022YFSH0027)
Corresponding author: ZHANG Xiang. E-mail: 20226016006@mails.imnu.edu.cn

Wang et al., 2012). When studying multiyear time series of vegetation cover, the characteristics of temporal and spatial changes in vegetation are very important. The ground survey vegetation data are relatively accurate (Haughian and Burton, 2018; Mugnani et al., 2019). However, field surveys can be limited by national politics and regional, economic, and other uncontrollable factors, so performing field surveys in a large area over multiple periods is difficult. To overcome this shortcoming, Earth observation remote sensing technology, can be used to detect target objects for long distance (Nigam and Bhatnagar, 2018). Because remote sensing is characteristically multiplatform, multilevel, multitemporal, multiband, and low price, remote sensing images can be used to monitor surface vegetation cover at microspatial scales and different time scales, thus enhancing local vegetation assessments (Oppenheimer, 1994). From the perspective of vegetation change research, Alcaraz-Segura et al. (Alcaraz-Segura et al., 2010) used Advanced Very High Resolution Radiometer (AVHRR) sensor data to evaluate trends in the normalized difference vegetation index (NDVI) from 1982–1999 in the Iberian Peninsula region (Spain and Portugal). Murray et al. (2018) used satellite remote sensing to assess spatial and functional changes in ecosystems and provided guidance on the use of satellite remote sensing data in ecosystem risk assessments. Other researchers (Liu et al., 2017b; Ahmed and Singh, 2020; Li et al., 2021) used Moderate-resolution Imaging Spectroradiometer (MODIS) image data to study habitat management based on local multiyear vegetation coverage, agricultural regional management and vegetation restoration change data. Therefore, MODIS NDVI imagery has become the main data source for researchers to conduct relevant vegetation monitoring in recent years (Beck et al., 2006; Lunetta et al., 2010; Yao et al., 2012).

At present, most scholars use the NDVI to assess the status of vegetation, and this index can represent the temporal and spatial changes in vegetation. Many methods have been proposed to monitor changes in vegetation growth. The main analytical methods include polynomial fitting (Xu et al., 2019), empirical mode decomposition (EEMD) (Ren et al., 2014) and neural network prediction (Carpenter et al., 1999). However, in the traditional linear trend fitting algorithm, the residual and standard deviation can not fully explain the results of linear fitting. These methods can be used to quickly estimate the trend and amplitude of NDVI changes, and multiyear interannual NDVI trends often ignore some details and sensitivity changes, which is insufficient for studies of NDVI time series. Moreover, this approach makes it difficult to predict future trends. Therefore, some researchers have studied multiyear trends using the autoregressive moving average (ARMA) to determine the significance of multiyear time series. The ARMA model can self-adapt to long-term time series, which is useful in certain applications. A strong positive correlation exists between sequence values at any adjacent point in time. Moreover, the high-frequency information in short time series can be used to reflect dynamic changes in vegetation.

Currently, some researchers use Sen's slope method (Sen, 1968) to study the overall trend of NDVI time series. However, this method can only be used to estimate the NDVI, and it is not sensitive to outliers and skewed distributions; moreover, the significance of the slope is not considered. As a result, the results lack statistical significance. Therefore, some researchers have combined the Mann-Kendall test (Shourov and Ishtiak, 2019) and Sen's slope method to evaluate the significance of the trends of interannual NDVI data (Gocic and Trajkovic, 2013; da Silva et al., 2015). This approach generates more information than the traditional trend method. However, the Mann-Kendall test and Sen's slope method ignore other characteristics and sensitive features of NDVI time series. High-frequency NDVI time series can reflect the entire process of vegetation change in a short time interval due to the diversity and uncertainty of the data (Friedl et al., 1995; de Jong et al., 2011; Ben Abbes et al., 2018). Some researchers have proposed novel approaches to vegetation change assessment. For example, breaks for additive season and trend (BFAST) (Verbesselt et al., 2010a) and vegetation change trackers (Huang et al., 2010) can be used to monitor long-term time series of vegetation changes (Forkel et al., 2013). The BFAST method can detect seasonal changes in the vegetation cycle and monitor long-term NDVI trends (Eastman et al., 2013; Forkel et al., 2015; Guo et al., 2021). Therefore, the internal cycle change in NDVI time series can be effectively revealed by comprehensively analysing the available detailed information.

In recent years, remote sensing research on vegetation changes and the corresponding influential factors in

cross-border areas between China and Mongolia at different time scales. In particular, little is known about the contribution of anthropogenic activities to vegetation changes in the Kherlen River Basin; such information plays an important role in local vegetation assessments and economic development related to animal husbandry. The growth and degradation of vegetation are affected by both natural and anthropogenic factors (Song et al., 2020; Xu et al., 2020; Kang et al., 2021). Many studies have shown that the relationship between a vegetation index and meteorological factors is mainly related to temperature and precipitation, that the selection of influential factors is inadequate, and that changes in the responses of different types of vegetation cover can lead to deviations in the conclusions (Ren et al., 2016; Chen et al., 2020). Furthermore, research on the impact of anthropogenic activities on vegetation is very limited. Researchers have used the residual analysis method to quantify the impact of anthropogenic activities on overall vegetation characteristics, but the theoretical formula is relatively simple, and it is difficult to obtain accurate results. Moreover, the factors that influence vegetation are complex and variable, and using a simple nonlinear correlation fitting is inadequate. To obtain the relative driving factors of NDVI from a multivariable perspective combined with climate, anthropogenic, land type and local terrain factor data, the geodetector approach (Qiao et al., 2019; Wang et al., 2019) can be used. With continuous changes in the ecological environment and land degradation, we selected the gross domestic product (GDP), land use type, number of livestock and population data as important indicators to measure anthropogenic activities (Crook et al., 2020; Caiyun et al., 2021).

Although some researchers have performed research on the NDVI and its related factors and considered the role of natural factors, information on the joint role of natural and anthropogenic factors is lacking, and relevant quantitative research is limited. Therefore, this study focused on the Kherlen River Basin from 2000–2020 as follows: 1) ARMA and BFAST were used to explore the stationarity of and detect the breakpoints in monthly NDVI data; 2) the spatial coefficient of variation (CV) was used to determine the trend and stability level of long-term NDVI time series in the entire study area; and 3) the effects of single and combined natural, anthropogenic and topographic factors on the NDVI were quantified using Geodetector. The results of this study could provide a strong theoretical reference for further improving grassland ecological restoration and management.

2 Materials and Methods

2.1 Study area

The boundary of the Kherlen River Basin is located at the southeastern end of Eurasia. The Kherlen River originates in the eastern part of Kent, Mongolia, flows through Mongolia from west to east, and then flows into Hulun Lake in Inner Mongolia, China. We divided the upper reaches, middle reaches, lower reaches and boundary of the Kherlen River Basin according to the administrative boundaries. As shown in Fig. 1, the main longitude and latitude are 107.5°E–117.5°E and 46.5°N–49.5°N, the altitude ranges from 483–2524 m, the topographic slope mainly fluctuations in the range of 5°–25°, the terrain is high in the west and low in the east, and the area is mainly composed of low mountains, hills, and grasslands. The climate is a typical temperate continental climate, with an annual average temperature of 0–3.2°C and average annual precipitation totalling 156.2–270.6 mm. The weather is variable, with four distinct seasons and periods of rain and high temperatures annually (Tsujimura et al., 2007). The total length of the river is 1264 km, and the drainage area is approximately 129 600 km^2 (including the drainage area of its tributaries and Hulun Lake). The total length in China is 206.44 km, and the drainage area is approximately 5486 km^2. The main vegetation community types are *Achnatherum splendens*, *Elymus dahuricus*, *Leymus chinensis* and *Hordeum brevibulatum* (Li et al., 2007).

2.2 Data and processing

The NDVI data were obtained from the MOD13A1 product with a 500 m spatial resolution, a 16-d temporal resolution and a monthly scale (https://lpdaacsvc.cr.usgs.gov/appeears/task/area). A year was defined as the period from January to December. The image data were preprocessed by Savitzky-Golay (S-G) filtering to eliminate noise, obtain long-term trends to the greatest extent and highlight local mutation information (Li et al., 2015; Nikonov et al., 2017; Zhu et al., 2017). The MODIS NDVI data that were S-G filtered were combined with the maximum values after using a mixed-

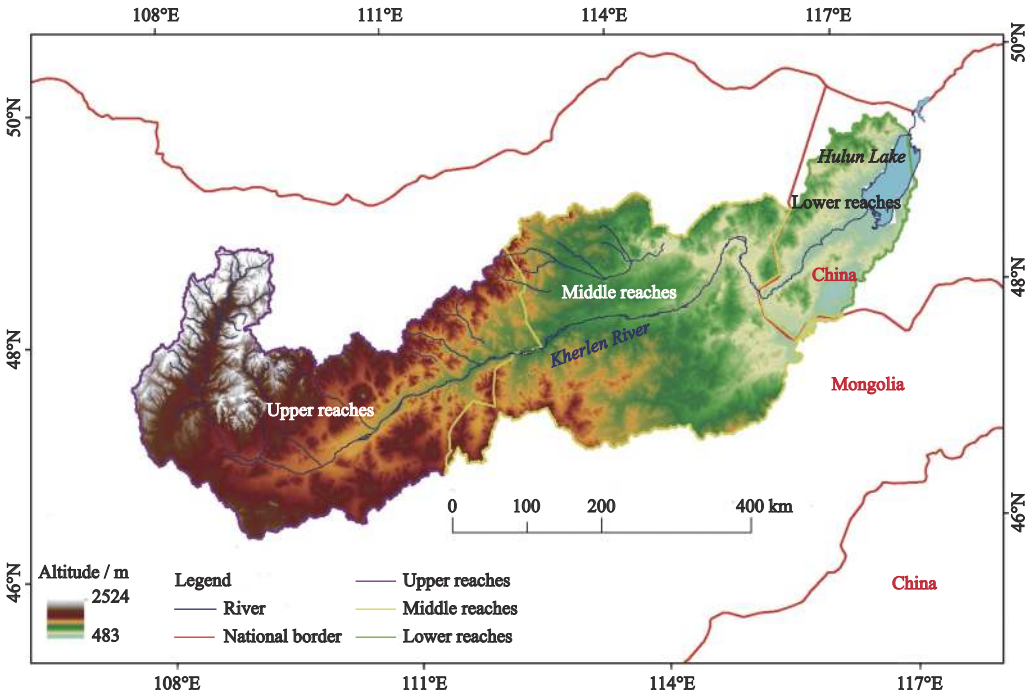

Fig. 1 Location and altitude of the Kherlen River Basin

pixel dichotomy model to effectively reduce the impacts of atmospheric, cloud and background parameters and to further obtain the interannual vegetation coverage.

The meteorological data were obtained from the official Copernicus climate data website (https://www.copernicus.eu/en). The reanalysis dataset ERA5 (spatial resolution: 0.1°) and the mean temperature and cumulative precipitation data were extracted from NetCDF format each month for the projection grid and resampled to obtain temperature and precipitation grid data with a projection and pixel size that were unified with those of the NDVI data.

Anthropogenic data were from the China-Mongolia Statistical Yearbook, including the quantity of livestock, the human population (People), and the gross domestic product (GDP) from 2000 to 2020 (http://tj.nmg.gov.cn/tjyw/jpsj/and http://www.1212.mn/). Considering that the relevant livestock population and GDP data have a certain joint, radiation effect on space, they are spatially interpolated by the inverse distance weighted (IDW) interpolation method, a portion of the data locations from each area are used as the test set, and the parameters are optimized by estimating the value of each location in the test set using the remainder locations. As the distance increases, the value of the prediction point becomes less affected by the discrete point (Myers, 1994). The sensitivity of the results to parameter values varies substantially, depending on local areas. According to the administrative division unit, we create 400 random points in the whole study area from which to extract the corresponding grid data.

The topographic data were obtained from ASTER-GDEM V1 imagery (https://www.gscloud.cn). An image mosaic was created to obtain a digital elevation model (DEM) with a spatial resolution of 30 m in the study area, and the terrain slope data were extracted from the DEM.

The data were preprocessed to meet the relevant accuracy requirements for this study. Table 1 shows the sources of data.

2.3 Methods

2.3.1 ARMA model

If a time series is stable, the mean and variance of the series will not change, and the ARMA model can be used for prediction. The ARMA model is a hybrid model that combines an autoregressive (AR) model and a moving average (MA) model (Hassan 2014; Shadab et al. 2019). The general form of the ARMA model is ARMA(p, q), where p and q represent the numbers of autoregressive AR terms and moving average MA terms, respectively. The ARMA modelling process can be summarized as selecting a model, estimating parameters and verifying the model. These three steps are

Table 1 Sources of data

Data	Time scale	Spatial scale	Data source
NDVI	2000–2020	500 m	MOD13A1 (https://lpdaacsvc.cr.usgs.gov/appeears/task/area)
Meteorological data	2000–2020	0.1°	Temperature, precipitation (https://www.copernicus.eu/en)
DEM	2009	30 m	ASTER-GDEM V1 (https://www.gscloud.cn)
Slope	2009	30 m	Extracted by DEM
Number of livestock	2000–2020	National	China-Mongolia Statistical Yearbook (http://tj.nmg.gov.cn/tjyw/jpsj/ and http://www.1212.mn/)
Human population (People)	2000–2020	National	China-Mongolia Statistical Yearbook (http://tj.nmg.gov.cn/tjyw/jpsj/ and http://www.1212.mn/)
Gross domestic product (GDP)	2000–2020	National	China-Mongolia Statistical Yearbook (http://tj.nmg.gov.cn/tjyw/jpsj/ and http://www.1212.mn/)

repeated, and the autocorrelation function (ACF) and partial autocorrelation function (PACF) are used to determine the parameter values until the optimal model is obtained. Durdu (2010) described this method in detail. The model form is defined as follows:

$$Y_t = \varphi_1 Y_{t-1} + \varphi_2 Y_{t-2} + \varphi_p Y_{t-p} + \theta_1 e_{t-1} + \theta_2 e_{t-2} + \theta_q e_{t-q} \quad (1)$$

where $\varphi_1 Y_{t-1} + \phi_2 Y_{t-2} + \varphi_p Y_{t-p}$ represents the AR model, the observation value of t is a linear combination of the previous p observation values, $\theta_1 e_{t-1} + \theta_2 e_{t-2} + \theta_q e_{t-q}$ represents the MA model, and the observation value of t is a linear combination of the previous q residual values.

2.3.2 *BFAST method*

BFAST can be used to decompose the seasonal terms, trend terms, and residual terms of multiyear time series into trends and breakpoints to capture the sensitive details of long-term time series (Verbesselt et al., 2010b). This BFAST method can be extended to mark the detected changes according to the parameter information for fitted piecewise linear models. This method is a flexible method that can deal with data gaps without requiring interpolation. The BFAST formulas are as follows:

$$Yt = Tt + St + et \quad (2)$$

$$Tt = \alpha_i + \beta_i t \quad (3)$$

$$St = \sum_{j=1}^{k} \gamma_i \sin\left(\frac{2\pi jt}{f} + \delta_j\right) \quad (4)$$

where Yt represents the NDVI time series from 2000 to 2020, Tt represents the trend analysis, α_i represents the intercept, and β_i represents the slope of the trend. This equation uses ordinary least squares regression to estimate the parameters α_i and β_i, where β_i is the slope of the time series segment. A t test was used to estimate the significance of each part of the trend for the time series segments, and β_i represents the interaction parameters of the regression. St represents the seasonal analysis, γ_i represents the amplitude, δ_j represents the phase harmonic term of the trend, f represents the number of observations per year, and et represents the other components.

2.3.3 *Coefficient of variation (CV) method*

As an important index of the degree of variation in multiyear spatiotemporal series, the CV can effectively measure the stability of multiyear interannual spatiotemporal vegetation changes (Chanda et al., 2018). The lower the CV is, the stronger the stability of interannual spatiotemporal vegetation changes is. The formula is

$$CV = \frac{1}{\overline{NDVI}} \sqrt{\frac{\sum_{i=1}^{n} \left(NDVI_i - \overline{NDVI}\right)^2}{n-1}} \quad (5)$$

where $NDVI$ represents the interannual average $NDVI$ from February 2000 to December 2020. In this study, the CV was used to represent the degree of interannual $NDVI$ variation over many years. The calculated CV results reflect the stability of the $NDVI$ per pixel in the study area from 2000 to 2020.

2.3.4 *Geodetector model*

Geodetector is a set of statistical methods used to detect spatial heterogeneity and reveal driving forces (Wang et al., 2019; Zhao et al., 2020; Jia et al., 2021). Geodetector detects the interactions between two factors based on dependent variables. The general method used to identify these interactions involves adding the product terms of two factors to a regression model to test for statistical significance. By calculating and comparing the q_{geo}

values of all individual factors, Geodetector can assess the interactions between the two selected factors.

$$q_{geo} = 1 - \frac{\sum_{h=1}^{L} N_h \sigma_h^2}{N\sigma^2} = 1 - \frac{SSW}{SST} \tag{6}$$

$$SSW = \sum_{h=1}^{L} N_h \sigma_h^2,\ SST = N\sigma^2 \tag{7}$$

where q_{geo} represents the measurement factor with the value ranges from 0 to 1. Specifically, the larger the value of q_{geo} is, the greater the impact on the spatial distribution of the NDVI is. In addition, h represents the division of the entire study area into several independent subareas, N_h and N represent the number of pixels in a subregion and the entire region, respectively, σ_h^2 and σ^2 represent the variance in a subregion and the entire region, respectively, and SSW and SST represent the sum of squares and the total sum of squares for the entire region, respectively.

F statistics can be used to determine the significant differences between the effects of two driving factors on the spatial distribution of dependent variables.

$$F = \frac{N_{x1} \times (N_{x2} - 1) SSW_{x1}}{N_{x2} \times (N_{x1} - 1) SSW_{x2}} \tag{8}$$

where N_{x1} and N_{x2} represent the sample size of the two factors and SSW_{x1} and SSW_{x2} represent the within-sum of squares originating from the two factors.

A t test was used to detect the influence of different factors that influence vegetation within a certain range. The formula is defined as follows:

$$t = \frac{\overline{Y}_{h=1} - \overline{Y}_{h=2}}{\left(\frac{\mathrm{Var}(Y_{h=1})}{n_{h=1}} + \frac{\mathrm{Var}(Y_{h=2})}{n_{h=2}}\right)^2} \tag{9}$$

where Y_h represents the average $NDVI$ pixel value for each subregion h, n_h represents the number of subregions, and Var represents the variance.

3 Results and Analyses

3.1 NDVI time series fitting and prediction analysis

With Statistical Product and Service Software Automatically (https://spssau.com/indexs.html), AR(5), ARMA (3,1), ARMA(2,2) and ARMA(3,1) corresponding formulas with the Akaike Information Criterion (AIC) and the Bayesian Information Criterion (BIC) (the lower the value is, the better it is) were used to obtain UB, MB, LB and BB results, respectively.

The corresponding formulas for the models are given as follows:

$$y_{UB}(t) = 0.215 + 1.227 \times y(t-1) - 0.203 \times y(t-2) - 0.088 \times y(t-3) + 0.014 \times y(t-4) - 0.143 \times y(t-5) \tag{10}$$

$$y_{MB}(t) = 0.201 + 1.981 \times y(t-1) - 1.17 \times y(t-2) + 0.123 \times y(t-3) - 0.826 \times \varepsilon(t-1) \tag{11}$$

$$y_{LB}(t) = 0.149 + 1.822 \times y(t-1) - 0.896 \times y(t-2) - 0.68 \times \varepsilon(t-1) - 0.125 \times \varepsilon(t-2) \tag{12}$$

$$y_{BB}(t) = 0.2 + 2.036 \times y(t-1) - 1.265 \times y(t-2) + 0.167 \times y(t-3) - 0.835 \times \varepsilon(t-1) \tag{13}$$

where $y_{UB}(t)$, $y_{MB}(t)$, $y_{LB}(t)$ and $y_{BB}(t)$ represent the ARMA time series results for UB, MB, LB and BB, respectively.

Through comprehensive analysis, it is concluded that the fitting values of the $y_{UB}(t)$, $y_{MB}(t)$, $y_{LB}(t)$ and $y_{BB}(t)$ models in Table 2 and Fig. 2 are close to the actual NDVI values, and long-term NDVI values can be established using the ARMA model. To evaluate the prediction performance of the model, the NDVI dataset is divided into a training set (Feb. 1, 2000 to Dec. 31, 2019) and a test set (Jan. 1, 2020 to Jun. 30, 2020). In Table 2, during the NDVI prediction period, the NDVI time

Table 2 Predicted NDVI time series in Jan.–Jun., 2020 by ARMA model for upper reaches, middle reaches, lower reaches and Kherlen River Basin

Forecast	Lag time1	Lag time 2	Lag time 3	Lag time 4	Lag time 5	Lag time 6	Lag time 7	Lag time 8	Lag time 9	Lag time 10	Lag time 11	Lag time 12
$y_{UB}(t)$ value	0.035	0.042	0.080	0.122	0.168	0.211	0.250	0.281	0.302	0.312	0.312	0.303
$y_{MB}(t)$ value	0.007	0.006	0.018	0.044	0.079	0.121	0.166	0.210	0.250	0.283	0.308	0.322
$y_{LB}(t)$ value	0.009	0.003	0.009	0.025	0.048	0.077	0.107	0.138	0.166	0.190	0.209	0.221
$y_{BB}(t)$ value	0.422	0.416	0.394	0.357	0.312	0.260	0.208	0.159	0.116	0.082	0.060	0.050

Notes: $y_{UB}(t)$ value, $y_{MB}(t)$ value, $y_{LB}(t)$ value and $y_{BB}(t)$ value represent predicted NDVI time series by ARMA model for upper reaches, middle reaches, lower reaches and Kherlen River Basin, respectively. Lag time 1–12 represent 12 periods of NDVI forecasting data

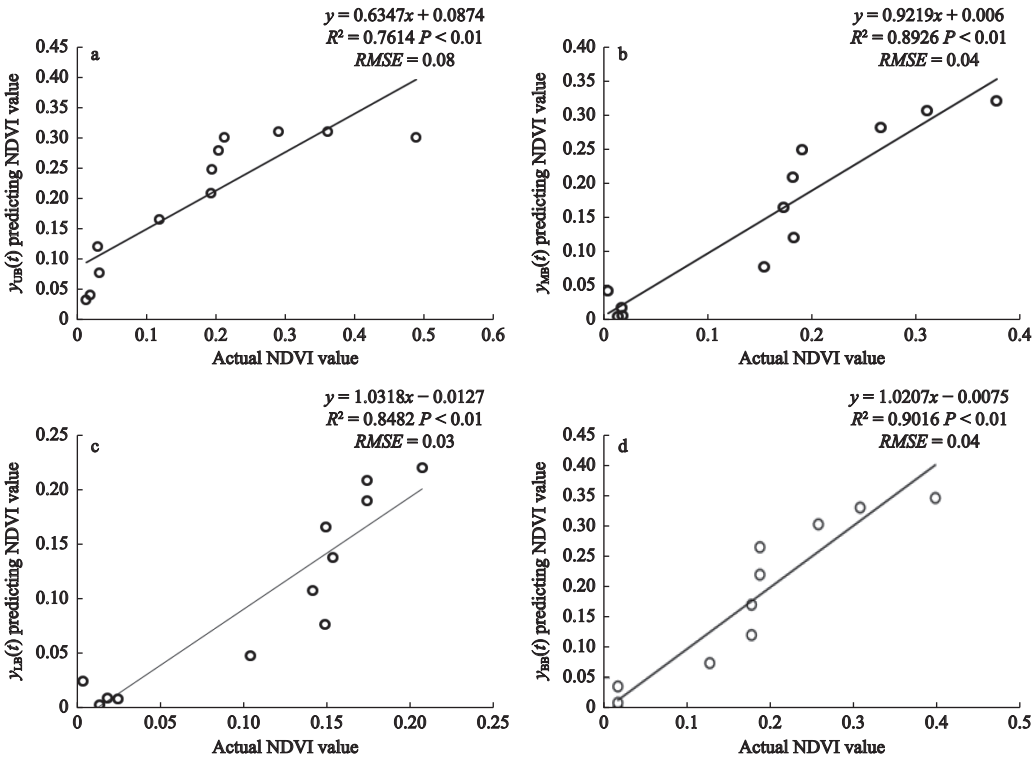

Fig. 2 (a) $y_{UB}(t)$, (b) $y_{MB}(t)$, (c) $y_{LB}(t)$ and (d) $y_{BB}(t)$ predicting NDVI value for upper reaches, middle reaches, lower reaches and Kherlen River Basin, respectively

series showed a decreasing trend. The ARMA model was used to obtain predictions over a period of 6 months, with a total of 12 periods of forecasting data. As shown in Figs. 2a–2d, the $y_{UB}(t)$, $y_{MB}(t)$, $y_{LB}(t)$ and $y_{BB}(t)$ models passed the white noise test, and the prediction results of all models were consistent with the actual NDVI values. It is worth noting that the evaluation index produced by the ARMA model is the best, but the predicted values exhibit little change. As shown in Figs. 2a–2d, the predicted values for the next 12 periods generally agree with the actual NDVI values, and the ARMA model yields an R^2 value of 0.76–0.90 ($P < 0.01$). Thus, the ARMA model can effectively predict the NDVI time series. Based on the above analysis, we conclude that although the NDVI fitting formulas used in the ARMA model vary for different regions, the NDVI prediction effects of the ARMA model in different regions are relatively similar.

3.2 NDVI time series decomposition analysis

Natural and anthropogenic factors can cause vegetation mutations at certain times. Therefore, we used BFAST to assess the monthly NDVI time series in different reaches of the Kherlen River Basin. As shown in Fig. 3, the NDVI fluctuated significantly from 2000 to 2020. Three break points in the monthly NDVI were observed in the upper reaches, middle reaches, and the entire boundary region of the basin, and no statistically significant increases in the NDVI were observed from 2000 to 2013 or from 2017 to 2020. These results suggest that the changes in the local NDVI were stable and minimally influenced by natural and anthropogenic factors. Furthermore, a significant decreasing trend was observed from 2013 to 2017. This result indicates that due to the joint influence of climate change and anthropogenic activities, the local vegetation degraded over these four years. As shown in Fig. 3c, complex and variable natural and anthropogenic factors led to a change in the number of NDVI breaks from 2000 to 2020. The NDVI exhibited five breakpoints in the lower reaches and a significant slowly decreasing trend from 2000–2004 and from 2013–2017. Notably, the ecological environment has been degraded, and the population has been increasing for a long time in the lower reaches. In other years, no significant decreasing trend was observed. As shown in Fig. 4, the long-term NDVI in the entire basin was calculated based on the BFAST algorithm. We divided 2013 and 2017 into two mutation points to explore the

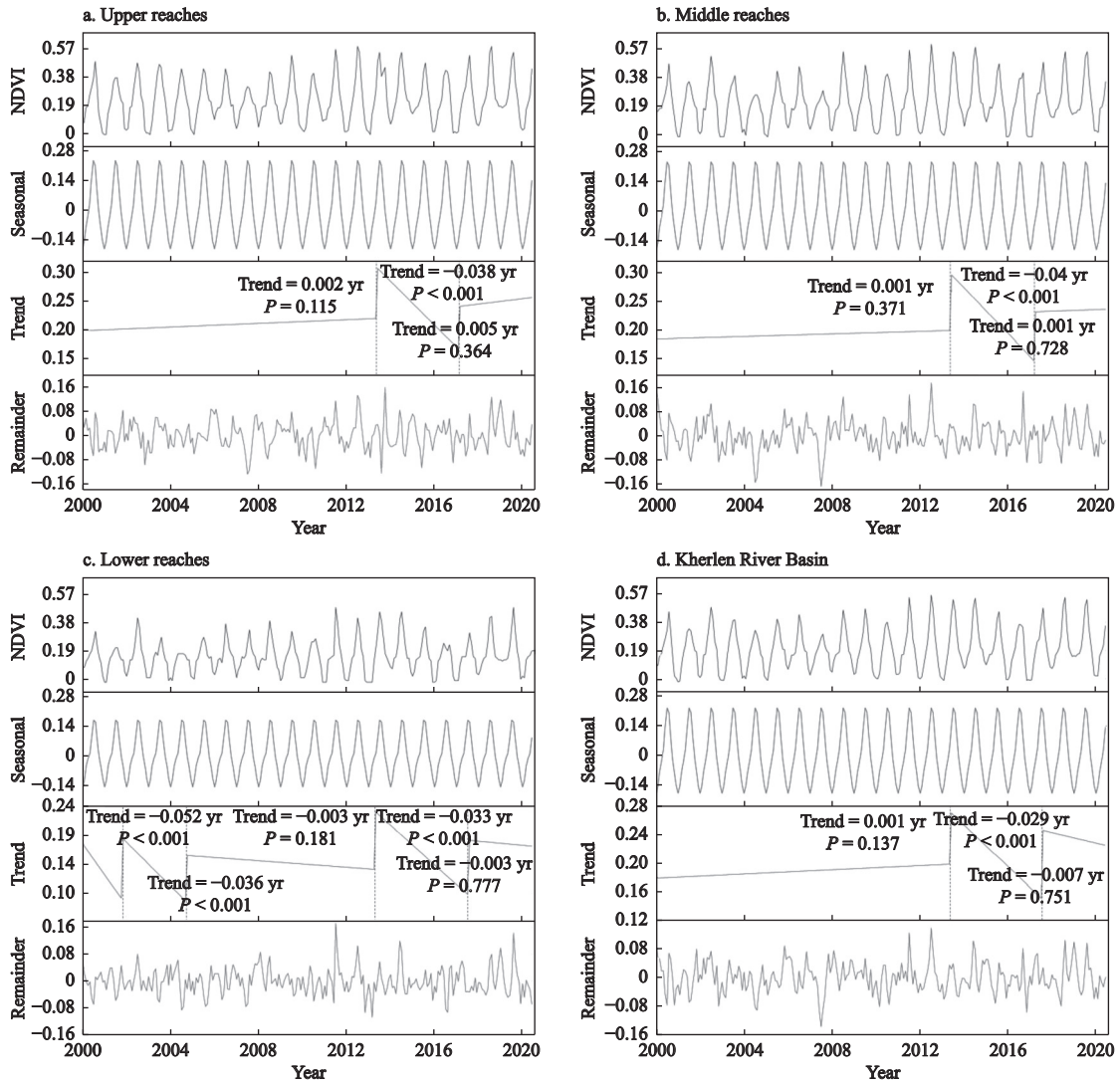

Fig. 3 Breaks for the additive season and trend (BFAST) model: the change in the monthly NDVI from 2000 to 2020. (a) Upper reaches, (b) middle reaches, (c) lower reaches and (d) Kherlen River Basin

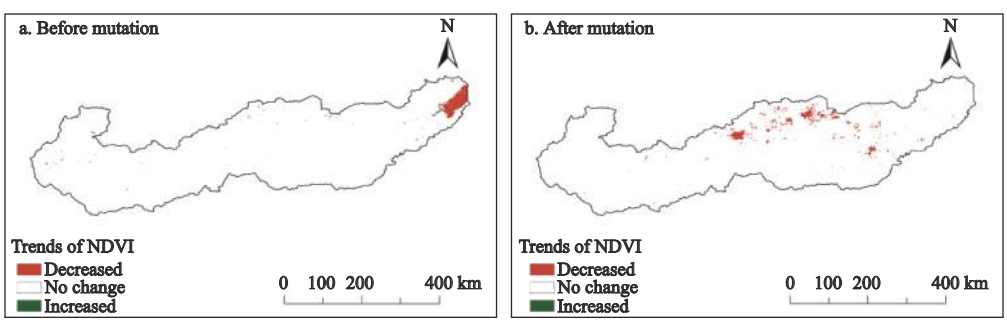

Fig. 4 Spatial distributions of trends before and after mutation in the Kherlen River Basin from 2000 to 2020

corresponding trend and the significance of the changes before and after mutations. We divided the NDVI trend from 2000 to 2020 into three classes: ‘increase’, ‘stable’ and ‘decrease’.

3.3 NDVI spatial stability analysis

We further explored the trend and stability level of the long-term NDVI time series in the entire study area. As shown in Fig. 5a–5b, from 2000 to 2020, the spatial

NDVI CV was relatively stable, mainly at the level of 0.01–0.07, with 45.14% of values between 0.04 and 0.05. Overall, the degree of variation in the spatial NDVI CV is highly variable and heterogeneously distributed throughout the study area. In the upper reaches of the Kherlen River Basin, the spatial CV remained at 0.01–0.05, which was slightly less than the CV of 0.05–0.07 in the middle reaches of the Kherlen River Basin. This result in the upper reaches, which may have been due to the reduced human impacts and no significant vegetation changes for many years, indicates that the local ecological environment is relatively stable and less affected by external interferences.

3.4 NDVI driving factor analysis

The factor detector results indicate the impact of each factor on the NDVI in the Kherlen River Basin, as expressed by the q_{geo} value (Fig. 6). The importance of the q_{geo} value varied in the basin, with a high q_{geo} value indicating an important impact on the NDVI. To determine the annual mean value from 2000 to 2020, we judge the abnormal value areas with 0 and negative values of

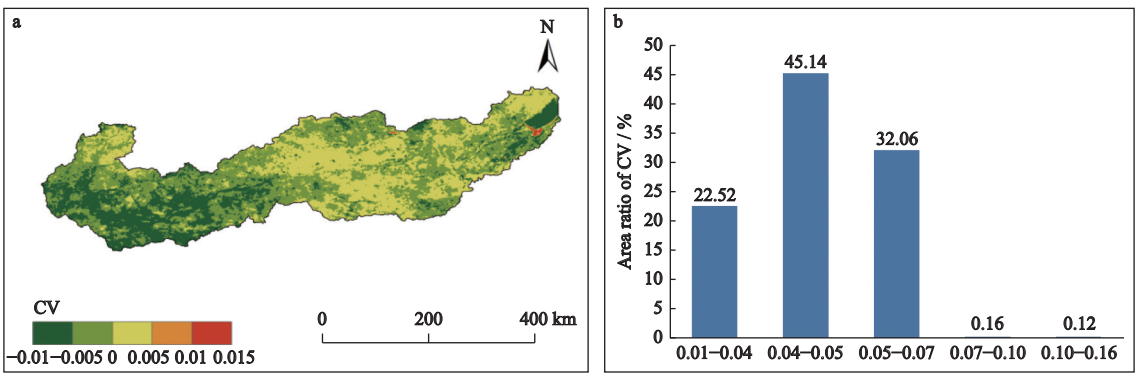

Fig. 5 NDVI results: (a) spatial map of the coefficient of variation (CV) and (b) statistical chart of the coefficient of variation in the Kherlen River Basin

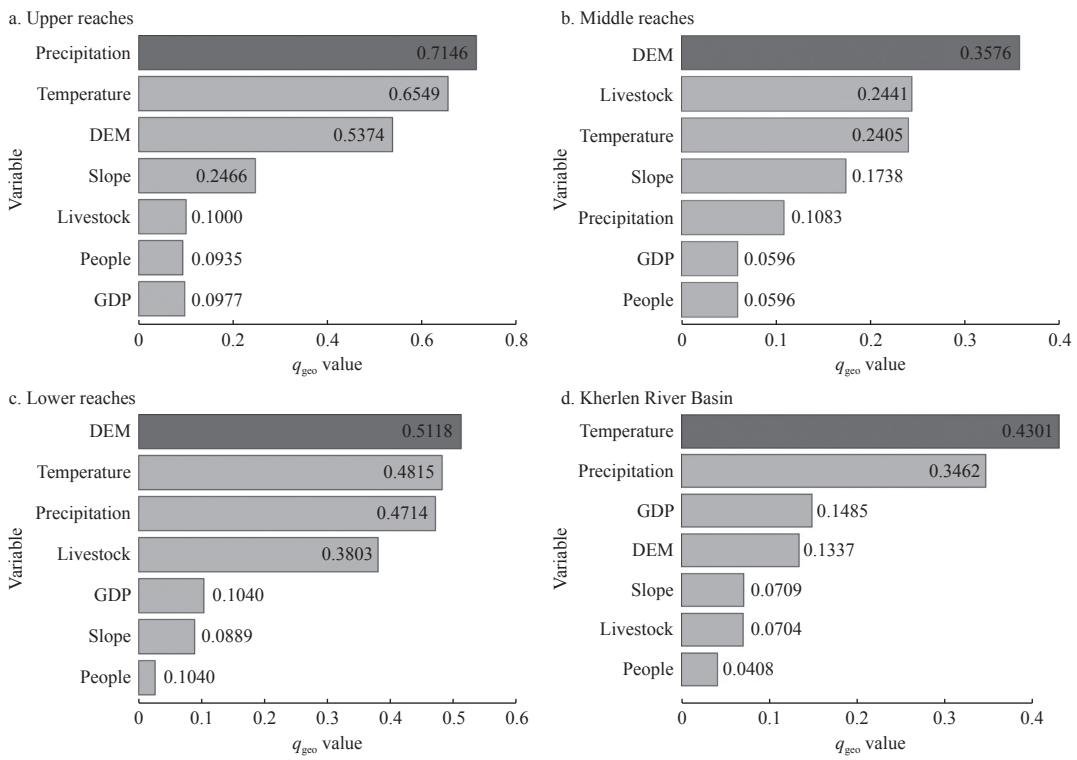

Fig. 6 NDVI results for each factor in the Kherlen River Basin from 2000 to 2020

MOD13A1 NDVI and exclude non-vegetation areas such as rocks, bare soil and waters. These corresponding grid data were considered outlier values and were removed. In the upper reaches, the q_{geo} value of precipitation was the highest, reaching 0.71, followed by those for temperature and the DEM. In the middle reaches, the q_{geo} value of the DEM was the highest, reaching 0.36, followed by those of livestock and temperature. In the lower reaches, the q_{geo} value of the DEM was the highest, reaching 0.51, followed by those of temperature and precipitation. In the entire basin, the q_{geo} value of temperature was the highest, reaching 0.43, followed by those of precipitation, GDP, the DEM, slope, livestock and human impact. Precipitation had an important impact of 0.35 on the NDVI, while GDP and the DEM had important impacts of 0.15 and 0.14 on the NDVI, respectively. Overall, the importance of local natural factors is greater than that of human factors. The other factors had q_{geo} values of less than 0.1, indicating that they had no important impacts on the NDVI.

The spatial pattern of NDVI change in the Kherlen River Basin is affected by multiple driving factors. Therefore, the interaction detector was used to determine the relationships among different driving factors (Fig. 7). The results show that the interactions among factors exhibited bilinear and nonlinear enhancement, with most interactions being nonlinear. Fig. 7b shows a weakening of unilinear variables. NDVI driving factors do not exist in isolation. The interaction between natural factors and human activities has an important composite effect on the growth of vegetation. The interaction detector results also reflect the interactions among components. The spatial distribution of the NDVI was affected differently by these interactions in the different

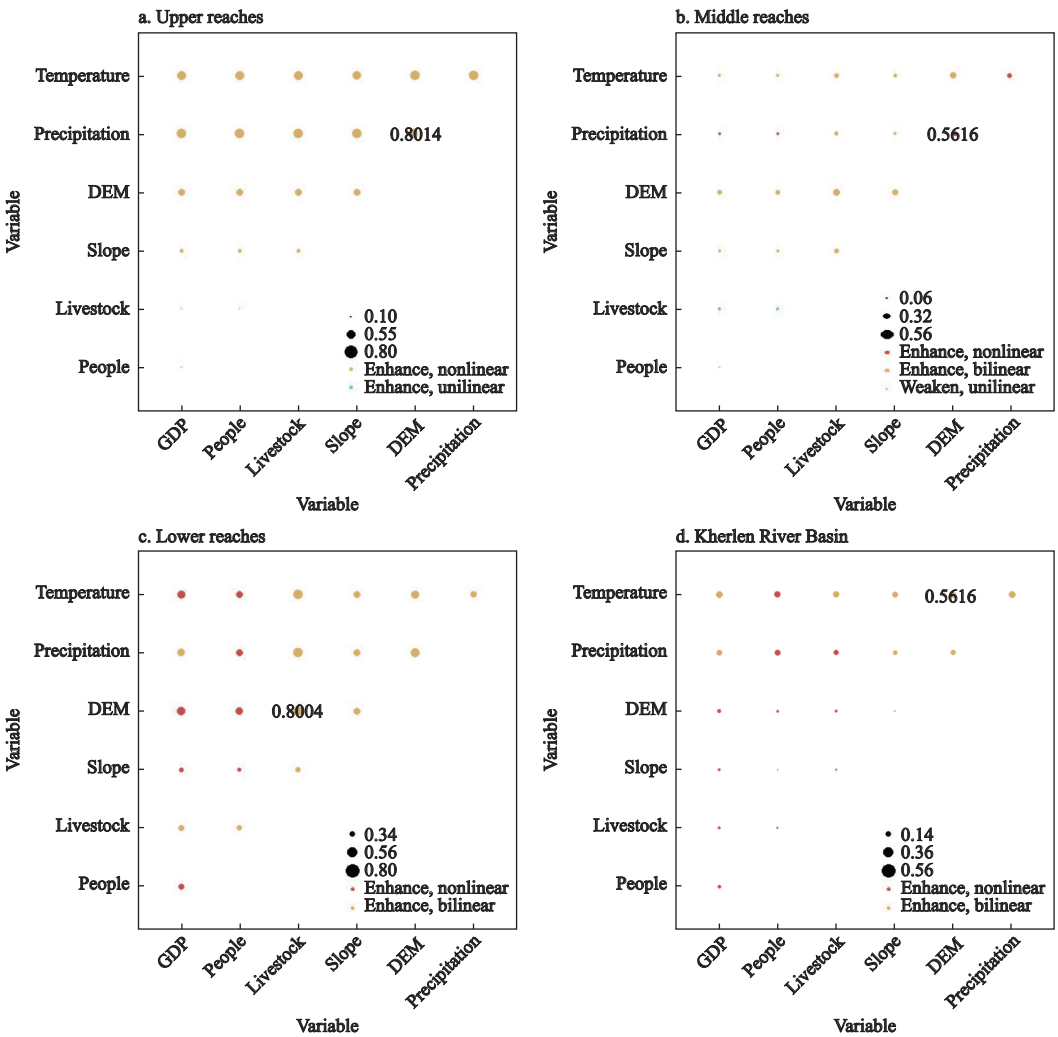

Fig. 7 Interaction detector results for each factor in the Kherlen River Basin from 2000 to 2020

reaches of the basin. In the upper and middle reaches, NDVI was influenced the most by the interaction between the DEM and precipitation, as shown in Figs. 7a, 7b. In the lower reaches, the NDVI was influenced the most by the interaction between the DEM and livestock, as shown in Fig. 7c. In the entire basin, the NDVI was influenced the most by the interaction between the DEM and temperature, with an effective factor of 0.56, as shown in Fig. 7d. Therefore, in the different reaches of the basin, the DEM displayed strong interactions with other factors. Natural factors, particularly temperature and precipitation, had a significant impact on the NDVI. Human factors, such as the GDP, quantity of livestock, and population, had minor impacts on the NDVI in the different reaches of the basin.

Ecological detectors can reflect the effects of different variables on the geographical distribution of the NDVI. The ecological detector results confirmed the most important influential factors and were used to assess the variabilities in their mechanisms. The ecological detector results (Fig. 8) show that natural factors, human factors, the DEM, and slope all had significantly different effects, demonstrating that while these factors all influenced the NDVI, the mechanisms that affected the development of vegetation in the different reaches of the basin varied. Notably, the impacts of natural and human factors on the NDVI showed significant differences. This finding demonstrates that natural and human factors had a major impact on the NDVI and interacted to modify the spatiotemporal distribution of the local NDVI. The effects of slope and livestock did not have a major influence on the spatiotemporal changes in

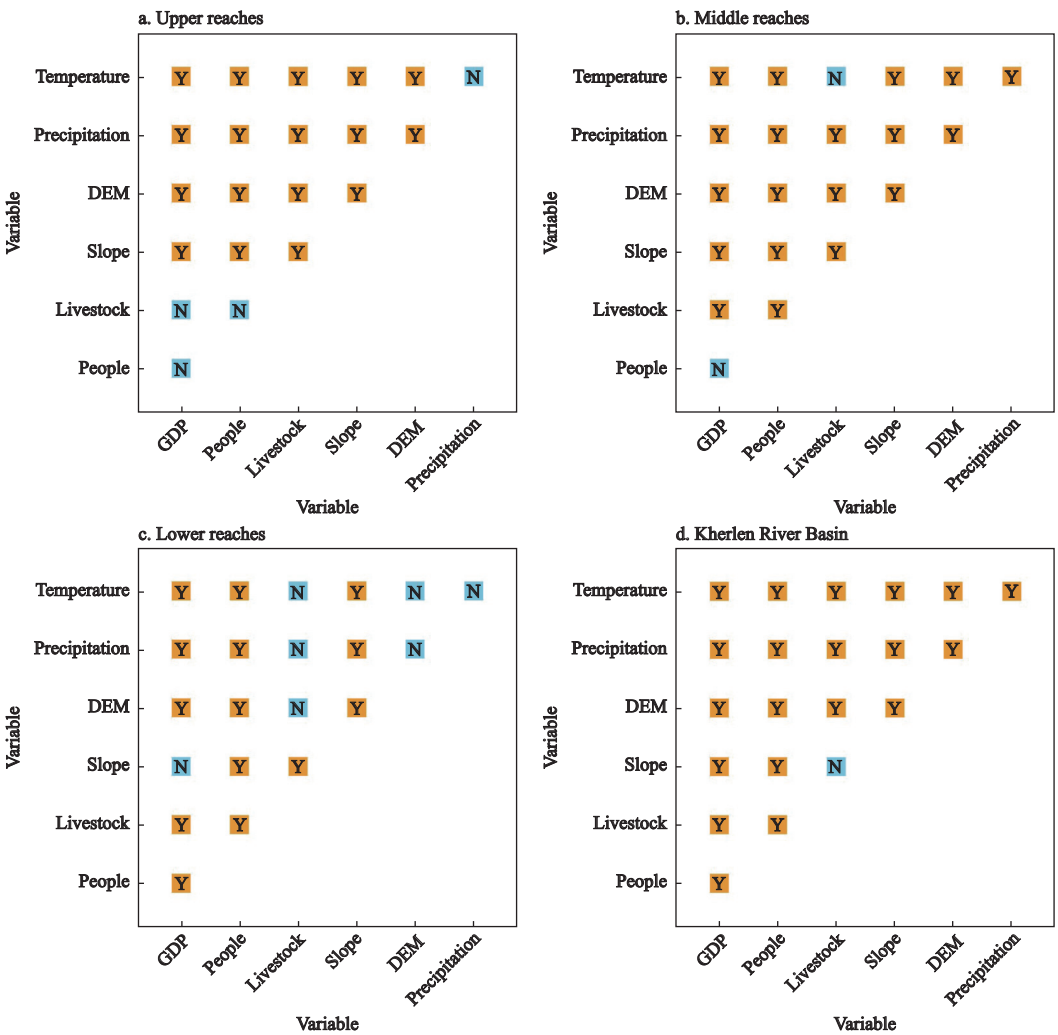

Fig. 8 Ecological detector results for each factor in the Kherlen River Basin from 2000 to 2020. Y labels and N labels indicate significant differences and no significant differences in the effects of the various factors on the spatial distribution of the NDVI

the NDVI.

4 Discussion

As a typical grassland cross-border river between China and Mongolia in eastern Asia, the Kherlen River originates in Kent, Mongolia. Due to the limited vegetation types, high vegetation stability and low river flow in the study area, spatial changes in the NDVI were not particularly obvious; notably, several inflection points were identified, and the NDVI was not easily affected by changes in the external conditions. However, the middle reaches of the Kherlen River Basin were shown to be vulnerable to changes in external conditions due to the joint actions of natural and human factors. Therefore, this part of the basin is the main area where the vegetation has rapidly changed and is not stable.

As part of the China-Russia-Mongolia Economic Corridor, the Kherlen River Basin provides Mongolia and neighbouring countries with high biodiversity value and plays an important role in maintaining the balance of local ecosystems, even though it is small compared with the main river basins in Russia and China. The overall joint management of cross-border river basins to maintain the natural resilience of the local ecosystems is the key to adapting to the rapidly changing climate. This study combined temperature and precipitation data and revealed the spatiotemporal changes in the vegetation coverage in the Kherlen River Basin from 2000 to 2020. The annual average vegetation coverage was maintained at 40%, with a relatively uniform spatial distribution and consistent stability. These findings are consistent with the conclusions of other scholars who have studied the spatial trends in the interannual vegetation coverage in China and performed spatial correlation analyses of temperature and precipitation (Guo et al., 2021). Some scholars have proposed that the stress effect of extreme weather conditions has an impact on the phenology of vegetation. In the future, we will explore the effects of extreme weather conditions on vegetation coverage.

Since ancient times, as a region of nomads in the north with heavy grazing and often continuous drought, the Kherlen River Basin has gradually become an area that is sensitive to global climate change (Kamimera and Lu, 2007). In recent years, China and Mongolia have formulated relevant vegetation restoration policies, and people have strengthened their awareness of environmental protection, which has gradually increased the local vegetation coverage. On the Chinese side, the Chinese government has vigorously promoted the return of farmland to forests and grassland and implemented the Three North Shelterbelt Systems project to recover the local environment. These measures have promoted the development of local grassland vegetation to a certain extent. At present, the general office of the State Council has issued several strategies to strengthen the protection and restoration of grasslands. On the Mongolian side, a small part of the floodplain in the Kherlen River Basin is protected by law. The prohibition of exploration and mining in river headwaters, watershed protected areas, and forest areas, which began in 2009, protects the most valuable landscape features of Mongolia, including river valleys, lake banks, forests, springs, important water flow accumulation areas, and other areas of mineral mining activities. From 2010 to 2012, the boundary of the nature reserve was redrawn with the participation of local communities. As a result, the rapid growth of Mongolia's GDP slowed. However, from 2000 to 2010, the establishment of the China-Mongolia-Russia Economic Corridor provided an unprecedented opportunity for Mongolia. As a pillar industry of Mongolia, animal husbandry needs to expand rapidly, and an increase in grazing will lead to a reduction in local grassland vegetation.

Vegetation is sensitive to changes in natural factors, which affect changes in the mutation years of the NDVI and the corresponding breakpoints. The q_{geo} value of natural factors is higher than that of human factors, mainly because in the Kherlen River Basin, temperature and precipitation are the main reasons for the changes in the NDVI. When the temperature and precipitation change abnormally, sudden changes in the local NDVI can occur. In different parts of the basin, the effects of various natural, human and topographic factors on the local NDVI also vary. In the upper reaches, changes in the hydrothermal conditions have had a considerable impact on local vegetation. In the middle and lower reaches, the varying altitude highly influences the local NDVI.

The NDVI is the most extensively used vegetation index worldwide. The leaf area index (Davi et al., 2006; Cristiano et al., 2014), vegetation coverage (Wu et al., 2014; Tang et al., 2020), chlorophyll content (Rulinda et al., 2011; Cristiano et al., 2014), and other relevant ve-

getation parameters are widely estimated using the NDVI. However, there are some drawbacks to using the NDVI to estimate the biomass and productivity of vegetation. First, the relationship between the NDVI and green biomass is nonlinear, and it can reach saturation in highly vegetated areas. The second constraint is that the NDVI primarily measures the spectral characteristics of vegetation and sometimes atmospheric noise and the soil background. To overcome the shortcomings of the NDVI, a new vegetation index kNDVI, which is based on machine learning and the kernel method, has been proposed. Compared with other indices, the kNDVI is more suitable for dealing with noise, saturation and complex phenology. The higher accuracy of the kNDVI is mainly associated with the consideration of the phenological cycle and the mitigation of noise and background effects (Camps-Valls et al., 2021).

In some cases, in the 16-day synthetic MOD13A1 NDVI data product, there was only one data source, and the spatial-temporal resolution was poor, which reduced the accuracy of time series breakpoint results. Data sources can be limited, and some time details are lost during the synthesis process. The two channels are unable to provide the distinctive patterns required for a well-classified image data due to a lack of complimentary band information (Useya and Chen, 2019). In future studies, the spatial details of GF-1 data can be fused with the spectral information of Sentinel-2 data. The high data accuracy is more suitable for crop information extraction in small-scale areas with complex ground object structures and fragmented plots. The results show that combining high spatial resolution with high-frequency time-series remote sensing data effectively improves the accuracy of ground object classification (Vasilakos et al., 2020). This process can provide large-scale and high-precision reference data for agricultural research (Shu et al., 2020) and the ecological environment protection of relevant areas. The driving mechanism of spatial vegetation changes should be further investigated in conjunction with climate change and ecological protection.

5 Conclusions

In view of the limited quantitative research on the ecological environment in the Kherlen River Basin in recent years, it is necessary to improve the understanding of local vegetation change. We analysed the MOD13A1 product with the ARMA and BFAST models and explored NDVI time series data from the Kherlen River Basin from 2000 to 2020. Notably, NDVI stability and related driving factors were investigated, and the ecological benefits of comprehensively considering the cross-border Kherlen River Basin were discussed. The main conclusions can be summarized as follows:

(1) The long-term NDVI research results show that NDVI fitting effect of ARMA model from 2000 to 2020, the correlation with R^2 between 0.76–0.90. Additionally, the accuracy of the ARMA model was high, with $RMSE$ = 0.03. For a specific period, the changes detected by BFAST show that the seasonal stability characteristics of the NDVI time series remained unchanged. A significant decreasing trend was observed from 2013 to 2017 in the entire study area.

(2) For the study period, the overall fluctuation in the NDVI in the entire study area can be described as follows: the CV mainly ranged from 0.01–0.07, and 45.14% of values ranged from 0.04–0.05. The results of this study show that the local ecological environment has been relatively stable, with little fluctuation in vegetation changes over time and limited external interference.

(3) Temperature and precipitation are the main driving factors of the NDVI in the Kherlen River Basin, and changes in local hydrothermal conditions will directly affect changes in the local NDVI. The differences among the interaction factors were mainly characterized as being due to nonlinear enhancement. Although natural, human, and topographic factors have certain effects on the growth of vegetation, significant differences exist in the interaction mechanisms associated with natural and human factors.

Our research provides reference for analyses of spatial distribution in local vegetation and ecological processes to the greatest extent possible. For NDVI time series, the ARMA method can overcome the shortcomings of singular models and improve the prediction accuracy. In future research, we will explore spatio-temporal NDVI data analysis. In addition, relevant data processing methods and model optimization should be considered to enhance the possibility of NDVI prediction.

Acknowledgements

We acknowledge the Extracting and Exploring Analys-

is Ready Samples (AρρEEARS) (https://lpdaacsvc.cr.usgs.gov/appeears/task/area) and the reanalysis dataset of ERA5-land (https://www.copernicus.eu/en), which provided NDVI and meteorological data. We thank the China and Mongolia government websites (http://tj.nmg.gov.cn/tjyw/jpsj/and http://www.1212.mn/) for providing statistical yearbook data. Furthermore, we thank the geospatial data cloud website (https://www.gscloud.cn) for providing topographical data. We thank the anonymous reviewers for their suggestions. We acknowledge the use of the BFAST and GD packages in R statistical software version 4.1.1, which provided the necessary algorithms, programs, and codes. Finally, we thank CHA Ersi, College of Geographic Science, Inner Mongolia Normal University, for providing data collation.

References

Ahmed T, Singh D, 2020. Probability density functions based classification of MODIS NDVI time series data and monitoring of vegetation growth cycle. *Advances in Space Research*, 66(4): 873–886. doi: 10.1016/j.asr.2020.05.004

Alcaraz-Segura D, Liras E, Tabik S et al., 2010. Evaluating the consistency of the 1982–1999 NDVI trends in the Iberian Peninsula across four time-series derived from the AVHRR sensor: LTDR, GIMMS, FASIR, and PAL-II. *Sensors*, 10(2): 1291–1314. doi: 10.3390/s100201291

Beck P S A, Atzberger C, Høgda K A et al., 2006. Improved monitoring of vegetation dynamics at very high latitudes: a new method using MODIS NDVI. *Remote Sensing of Environment*, 100(3): 321–334. doi: 10.1016/j.rse.2005.10.021

Ben Abbes A, Bounouh O, Farah I R et al., 2018. Comparative study of three satellite image time-series decomposition methods for vegetation change detection. *European Journal of Remote Sensing*, 51(1): 607–615. doi: 10.1080/22797254.2018.1465360

Caiyun G, Dongsheng Z, Du Z et al., 2021. Effects of grazing on the grassland vegetation community characteristics in Inner Mongolia. *Journal of Resources and Ecology*, 12(3): 319–331. doi: 10.5814/j.issn.1674-764x.2021.03.002

Camps-Valls G, Campos-Taberner M, Moreno-Martínez Á et al., 2021. A unified vegetation index for quantifying the terrestrial biosphere. *Science Advances*, 7(9): eabc7447. doi: 10.1126/sciadv.abc7447

Carpenter G A, Gopal S, Macomber S et al., 1999. A neural network method for efficient vegetation mapping. *Remote Sensing of Environment*, 70(3): 326–338. doi: 10.1016/S0034-4257(99)00051-6

Chanda S, Kanke Y, Dalen M et al., 2018. Coefficient of variation from vegetation index for sugarcane population and stalk evaluation. *Agrosystems, Geosciences & Environment*, 1: 1–9, 180016. doi: 10.2134/age2018.07.0016

Chen M L, Jin J L, Ning S W et al., 2020. Early warning method for regional water resources carrying capacity based on the logical curve and aggregate warning index. *International Journal of Environmental Research and Public Health*, 17(7): 2206. doi: 10.3390/ijerph17072206

Cristiano P M, Madanes N, Campanello P I et al., 2014. High NDVI and potential canopy photosynthesis of South American subtropical forests despite seasonal changes in leaf area index and air temperature. *Forests*, 5(2): 287–308. doi: 10.3390/f5020287

Crook D R, Robinson B E, Li P, 2020. The impact of snowstorms, droughts and locust outbreaks on livestock production in Inner Mongolia: anticipation and adaptation to environmental shocks. *Ecological Economics*, 177: 106761. doi: 10.1016/j.ecolecon.2020.106761

da Silva R M, Santos C A G, Moreira M et al., 2015. Rainfall and river flow trends using Mann-Kendall and Sen's slope estimator statistical tests in the Cobres River basin. *Natural Hazards*, 77(2): 1205–1221. doi: 10.1007/s11069-015-1644-7

Davi H, Soudani K, Deckx T et al., 2006. Estimation of forest leaf area index from SPOT imagery using NDVI distribution over forest stands. *International Journal of Remote Sensing*, 27(5): 885–902. doi: 10.1080/01431160500227896

de Jong R, de Bruin S, de Wit A et al., 2011. Analysis of monotonic greening and browning trends from global NDVI time-series. *Remote Sensing of Environment*, 115(2): 692–702. doi: 10.1016/j.rse.2010.10.011

Durdu Ö F, 2010. Application of linear stochastic models for drought forecasting in the Büyük Menderes River Basin, western Turkey. *Stochastic Environmental Research and Risk Assessment*, 24(8): 1145–1162. doi: 10.1007/s00477-010-0366-3

Eastman J R, Sangermano F, Machado E A et al., 2013. Global trends in seasonality of normalized difference vegetation index (NDVI), 1982–2011. *Remote Sensing*, 5(10): 4799–4818. doi: 10.3390/rs5104799

Eisavi V, Homayouni S, Yazdi A M et al., 2015. Land cover mapping based on random forest classification of multitemporal spectral and thermal images. *Environmental Monitoring and Assessment*, 187(5): 291. doi: 10.1007/s10661-015-4489-3

Forkel M, Carvalhais N, Verbesselt J et al., 2013. Trend change detection in NDVI time series: effects of inter-annual variability and methodology. *Remote Sensing*, 5(5): 2113–2144. doi: 10.3390/rs50521131

Forkel M, Migliavacca M, Thonicke K et al., 2015. Codominant water control on global interannual variability and trends in land surface phenology and greenness. *Global Change Biology*, 21(9): 3414–3435. doi: 10.1111/gcb.12950

Friedl M A, Davis F W, Michaelsen J et al., 1995. Scaling and uncertainty in the relationship between the NDVI and land surface biophysical variables: an analysis using a scene simulation model and data from FIFE. *Remote Sensing of Environment*, 54(3): 233–246. doi: 10.1016/0034-4257(95)00156-5

Gocic M, Trajkovic S, 2013. Analysis of changes in meteorolo-

gical variables using Mann-Kendall and Sen's slope estimator statistical tests in Serbia. *Global and Planetary Change*, 100: 172–182. doi: 10.1016/j.gloplacha.2012.10.014

Gottfried M, Pauli H, Futschik A et al., 2012. Continent-wide response of mountain vegetation to climate change. *Nature Climate Change*, 2(2): 111–115. doi: 10.1038/nclimate1329

Goward S N, Xue Y K, Czajkowski K P, 2002. Evaluating land surface moisture conditions from the remotely sensed temperature/vegetation index measurements: an exploration with the simplified simple biosphere model. *Remote Sensing of Environment*, 79(2−3): 225–242. doi: 10.1016/S0034-4257(01)00275-9

Guo E L, Wang Y F, Wang C L et al., 2021. NDVI indicates long-term dynamics of vegetation and its driving forces from climatic and anthropogenic factors in Mongolian Plateau. *Remote Sensing*, 13(4): 688. doi: 10.3390/rs13040688

Hassan J, 2014. ARIMA and regression models for prediction of daily and monthly clearness index. *Renewable Energy*, 68: 421–427. doi: 10.1016/j.renene.2014.02.016

Haughian S R, Burton P J, 2018. Microclimate differences above ground-layer vegetation in lichen-dominated pine forests of north-central British Columbia. *Agricultural and Forest Meteorology*, 249: 100–106. doi: 10.1016/j.agrformet.2017.11.029

Huang C Q, Goward S N, Masek J G et al., 2010. An automated approach for reconstructing recent forest disturbance history using dense Landsat time series stacks. *Remote Sensing of Environment*, 114(1): 183–198. doi: 10.1016/j.rse.2009.08.017

Jia W J, Wang M F, Zhou C H et al., 2021. Analysis of the spatial association of geographical detector-based landslides and environmental factors in the southeastern Tibetan Plateau, China. *PLoS ONE*, 16(5): e0251776. doi: 10.1371/journal.pone.0251776

Juliana Useya, Chen Shengbo, 2019. Exploring the potential of mapping cropping patterns on smallholder scale croplands using Sentinel-1 SAR data. *Chinese Geographical Science*, 20(4): 626–639. doi: 10.1007/s11769-019-1060-0

Kamimera H, Lu M J, 2007. Water balance of the Kherlen River basin, eastern Mongolia. *Proceedings of Hydraulic Engineering*, 51: 397–402. doi: 10.2208/prohe.51.397

Kang Y, Guo E L, Wang Y F et al., 2021. Monitoring vegetation change and its potential drivers in Inner Mongolia from 2000 to 2019. *Remote Sensing*, 13(17): 3357. doi: 10.3390/rs13173357

Kim S R, Lee W K, Kwak D A et al., 2011. Forest cover classification by optimal segmentation of high resolution satellite imagery. *Sensors*, 11(2): 1943–1958. doi: 10.3390/s110201943

Li D Q, Lu D S, Zhao Y et al., 2021. Spatial patterns of vegetation coverage change in giant panda habitat based on MODIS time-series observations and local indicators of spatial association. *Ecological Indicators*, 124: 107418. doi: 10.1016/j.ecolind.2021.107418

Li Ming, Shen Runping, Wang Di et al., 2015. Reconstruction of MODIS-NDVI using S-G filtering based on pixel quality analysis. *Journal of Ecology and Rural Environment*, 31(3): 425–431. (in Chinese)

Li S G, Romero-Saltos H, Tsujimura M et al., 2007. Plant water sources in the cold semiarid ecosystem of the upper Kherlen River catchment in Mongolia: a stable isotope approach. *Journal of Hydrology*, 333(1): 109–117. doi: 10.1016/j.jhydrol.2006.07.020

Liu R G, Shang R, Liu Y et al., 2017a. Global evaluation of gap-filling approaches for seasonal NDVI with considering vegetation growth trajectory, protection of key point, noise resistance and curve stability. *Remote Sensing of Environment*, 189: 164–179. doi: 10.1016/j.rse.2016.11.023

Liu X F, Jiang W G, Li J et al., 2017b. Evaluation of the vegetation coverage resilience in areas damaged by the Wenchuan earthquake based on MODIS-EVI data. *Sensors*, 17(2): 259. doi: 10.3390/s17020259

Lunetta R S, Shao Y, Ediriwickrema J et al., 2010. Monitoring agricultural cropping patterns across the Laurentian Great Lakes Basin using MODIS-NDVI data. *International Journal of Applied Earth Observation and Geoinformation*, 12(2): 81–88. doi: 10.1016/j.jag.2009.11.005

Mugnani M P, Robertson K M, Miller D L et al., 2019. Longleaf pine patch dynamics influence ground-layer vegetation in old-growth pine Savanna. *Forests*, 10(5): 389. doi: 10.3390/f10050389

Murray N J, Keith D A, Bland L M et al., 2018. The role of satellite remote sensing in structured ecosystem risk assessments. *Science of the Total Environment*, 619–620: 249–257. doi: 10.1016/j.scitotenv.2017.11.034

Myers D E, 1994. Spatial interpolation: an overview. *Geoderma*, 62: 17–28. doi: 10.1016/0016-7061(94)90025-6

Nigam S K, Bhatnagar V, 2018. The systems biology of uric acid transporters: the role of remote sensing and signaling. *Current Opinion in Nephrology and Hypertension*, 27(4): 305–313. doi: 10.1097/MNH.0000000000000427

Nikonov A V, Davletshin R V, Iakovleva N I et al., 2017. Savitzky-Golay filtering of the spectral sensitivity of photodetector arrays. *Journal of Communications Technology and Electronics*, 62(9): 1048–1052. doi: 10.1134/S1064226917090170

Oppenheimer C, 1994. Discussion meeting on natural hazard assessment and mitigation: the unique role of remote sensing, the Royal Society, London. *Disasters*, 18(3): 294–297. doi: 10.1111/j.1467-7717.1994.tb00316.x

Qiao P W, Yang S C, Lei M et al., 2019. Quantitative analysis of the factors influencing spatial distribution of soil heavy metals based on geographical detector. *Science of the Total Environment*, 664: 392–413. doi: 10.1016/j.scitotenv.2019.01.310

Ren C F, Guo P, Li M et al., 2016. An innovative method for water resources carrying capacity research-Metabolic theory of regional water resources. *Journal of Environmental Management*, 167: 139–146. doi: 10.1016/j.jenvman.2015.11.033

Ren H, Wang Y L, Huang M Y et al., 2014. Ensemble empirical mode decomposition parameters optimization for spectral distance measurement in hyperspectral remote sensing data. *Re-*

mote Sensing, 6(3): 2069–2083. doi: 10.3390/rs6032069

Rulinda C M, Bijker W, Stein A, 2011. The chlorophyll variability in Meteosat derived NDVI in a context of drought monitoring. *Procedia Environmental Sciences*, 3: 32–37. doi: 10.1016/j.proenv.2011.02.007

Sen P K, 1968. Estimates of the regression coefficient based on Kendall's Tau. *Journal of the American Statistical Association*, 63: 1379–1389. doi: 10.1080/01621459.1968.10480934

Shadab A, 2019. Box–Jenkins multiplicative ARIMA modeling for prediction of solar radiation: a case study. *International Journal of Energy and Water Resources*, 3: 305–318. doi: 10.1007/s42108-019-00037-5

Shourov M M, Ishtiak M, 2019. pyMannKendall: a python package for non parametric Mann Kendall family of trend tests. *Journal of Open Source Software*, 4(39): 1556. doi: 10.21105/joss.01556

Shu M, Zhou L, Gu X et al., 2020. Monitoring of maize lodging using multi-temporal Sentinel-1 SAR data. *Advances in Space Research*, 65: 470–480. doi: 10.1016/j.asr.2019.09.034

Song Y Z, Wang J F, Ge Y et al., 2020. An optimal parameters-based geographical detector model enhances geographic characteristics of explanatory variables for spatial heterogeneity analysis: cases with different types of spatial data. *GIScience & Remote Sensing*, 57(5): 593–610. doi: 10.1080/15481603.2020.1760434

Tang L, He M Z, Li X R, 2020. Verification of fractional vegetation coverage and NDVI of desert vegetation via UAVRS technology. *Remote Sensing*, 12(11): 1742. doi: 10.3390/rs12111742

Tsujimura M, Abe Y, Tanaka T et al., 2007. Stable isotopic and geochemical characteristics of groundwater in Kherlen River basin, a semi-arid region in eastern Mongolia. *Journal of Hydrology*, 333(1): 47–57. doi: 10.1016/j.jhydrol.2006.07.026

Vasilakos C, Kavroudakis D, Georganta A. 2020. Machine learning classification ensemble of multitemporal Sentinel-2 images: The case of a mixed mediterranean ecosystem. *Remote Sensing*, 12: 2005. doi: 10.3390/rs12122005.

Verbesselt J, Hyndman R, Newnham G et al., 2010a. Detecting trend and seasonal changes in satellite image time series. *Remote Sensing of Environment*, 114(1): 106–115. doi: 10.1016/j.rse.2009.08.014

Verbesselt J, Hyndman R, Zeileis A et al., 2010b. Phenological change detection while accounting for abrupt and gradual trends in satellite image time series. *Remote Sensing of Environment*, 114(12): 2970–2980. doi: 10.1016/j.rse.2010.08.003

Wang L, Dronova I, Gong P et al., 2012. A new time series vegetation-water index of phenological-hydrological trait across species and functional types for Poyang Lake wetland ecosystem. *Remote Sensing of Environment*, 125: 49–63. doi: 10.1016/j.rse.2012.07.003

Wang W, Samat A, Abuduwaili J, 2019. Geo-detector based spatio-temporal variation characteristics and driving factors analysis of NDVI in Central Asia. *Remote Sensing for Land & Resources*, 31(4): 32–40. (in Chinese). doi: 10.6046/gtzyyg.2019.04.05

Wu D H, Wu H, Zhao X et al., 2014. Evaluation of spatiotemporal variations of global fractional vegetation cover based on GIMMS NDVI data from 1982 to 2011. *Remote Sensing*, 6(5): 4217–4239. doi: 10.3390/rs6054217

Xu L L, Yu G M, Tu Z F et al., 2020. Monitoring vegetation change and their potential drivers in Yangtze River Basin of China from 1982 to 2015. *Environmental Monitoring and Assessment*, 192(10): 642. doi: 10.1007/s10661-020-08595-6

Xu X J, Liu H Y, Lin Z S et al., 2019. Relationship of abrupt vegetation change to climate change and ecological engineering with multi-timescale analysis in the Karst Region, Southwest China. *Remote Sensing*, 11(13): 1564. doi: 10.3390/rs11131564

Yao J, He X Y, Li X Y et al., 2012. Monitoring responses of forest to climate variations by MODIS NDVI: a case study of Hun River upstream, northeastern China. *European Journal of Forest Research*, 131(3): 705–716. doi: 10.1007/s10342-011-0543-z

Zhao Y J, Deng Q Y, Lin Q et al., 2020. Cadmium source identification in soils and high-risk regions predicted by geographical detector method. *Environmental Pollution*, 263: 114338. doi: 10.1016/j.envpol.2020.114338

Zhu G F, Zhu H Q, Yang C H et al., 2017. Improved Savitzky-Golay filtering algorithm for measuring a pharmaceutical vial's oxygen content based on wavelength modulation spectroscopy. *Journal of Optical Technology*, 84(5): 355–359. doi: 10.1364/JOT.84.000355